



UNIVERSITÀ DEGLI STUDI DI MILANO
FACOLTÀ DI SCIENZE E TECNOLOGIE

Bachelor's Degree in Physics

**Next-to-Leading Order QCD Corrections to Scattering Processes Using
 θ -Parameters in the Nested Soft-Collinear Subtraction Scheme**

Supervisor:
Prof. Raoul Horst Röntsch

Student:
Lucrezia Bioni
Matr.: 13655A

Academic Year 2024–2025

Abstract

Quantum Chromodynamics (QCD) corrections at next-to-leading order (NLO) are an essential component of high-precision theoretical predictions in high-energy particle physics. The nested soft-collinear subtraction (NSC) scheme provides an established framework for computing these corrections, offering an efficient method for handling infrared (IR) divergences through a nested factorization of soft and collinear singularities. This approach ensures proper cancellation of divergences. In this work, we focus on hadronic scattering processes and we extend the NSC framework by implementing θ -parameters, which systematically restrict the subtraction procedure to the singular, unresolved regions of phase space. This refinement is designed to further enhance the scheme's numerical stability and computational efficiency by optimizing the treatment of IR-sensitive contributions.

Contents

1	Introduction	1
1.1	The Standard Model	1
1.2	Collider physics	1
1.3	QCD and hard scattering processes	2
1.4	Hadronic cross-section and factorization theorem	2
1.5	Partonic cross-section	5
1.6	Infrared poles and their cancellation	7
2	NLO QCD corrections in the NSC Subtraction Scheme	9
2.1	Properties of Soft and Collinear partons	9
2.2	Why a subtraction method	10
2.3	Soft and Collinear operators	11
2.4	Modularity of the scheme	12
2.5	Soft limit	13
2.6	Collinear and Soft-Collinear limits	15
2.6.1	Initial state	16
2.6.2	Final state	19
2.7	Cancellation of poles	20
3	NLO QCD corrections with θ-parameters in the NSC Subtraction Scheme	21
3.1	Draft	21
	Appendices	23
A	Useful definitions	25
A.1	Constants	25
A.2	Partitions at NLO	25
A.3	Splitting functions	26
	Bibliography	28

Introduction

§1.1 The Standard Model

As Aristotle stated, women and men began to philosophize due to wonder. From antiquity, a profound sense of astonishment towards the natural world has driven humans to investigate phenomenological reality. This drive is so profound and innate in humanity that – starting with the first philosophers, called “Pre-Socratics” or “natural philosophers” – it led them to inquire into the nature of the “archè” ($\acute{\alpha}\rho\chi\eta$), the primordial principle and fundamental constituent underlying all of nature. This enduring pursuit of fundamental knowledge evolved through the centuries and, in the last one, culminated in the experimental discovery of a multitude of subatomic particles. Their proliferation was such that it prompted the noted physicist Enrico Fermi to remark: “If I could remember the names of all these particles, I’d be a botanist”. This apparent complexity, however, has been successfully resolved through the development of a robust theoretical framework that classifies these particles and describes their interactions via gauge theories: the Standard Model (SM).

The SM is formulated within the mathematical framework of Quantum Field Theory (QFT), which unifies the principles of Quantum Mechanics and Special Relativity to describe phenomena at high energies, or equivalently, subatomic scales. Its predictions have been rigorously tested and confirmed by experiments, most notably with the discovery of the Higgs boson in 2012. Despite its success, there are significant efforts to discover Physics beyond the SM. This is driven not only by the natural attempt at falsification that should be applied to every scientific theory, but also by several phenomena that the model cannot explain. These include the existence of dark matter and dark energy, the observed matter-antimatter asymmetry, and the origin of neutrino masses [13].

§1.2 Collider physics

One of the principal methods of research in high-energy physics is collider physics [5]. Using colliders, it is possible to artificially accelerate particles and to reach extremely high center-of-mass energy. Operating at the energy frontier is crucial: higher-energy collisions enable events with greater momentum transfer and energy deposition. These events are essential because concentrating significant energy within a tiny volume allows us to excite new, heavy elementary particles from the vacuum, and study their properties. Experiments at the energy frontier are conducted at the Large Hadron Collider (LHC) at CERN: in a 27-kilometer ring,

proton beams collide at a center-of-mass energy of approximately 13.6 TeV. Although these energy scales have allowed us to study the known fundamental interactions – with the exception of gravity – in great detail, they have not been sufficient for the discovery of new particles. Since increasing the energy of the colliding particles is not feasible with existing technology, the focus of collider experiments in the next decade will shift towards higher experimental precision. This precision is crucial for refining our understanding of the Standard Model (SM), especially the properties of the Higgs boson: in fact, it is the agent of electroweak (EW) symmetry breaking, which is a fundamental component of the theory. Moreover, precision measurements serve as a powerful probe for new physics, which may reveal itself as subtle deviations from SM predictions in processes involving only known particles. However, testing the Standard Model with experimental results necessitates reliable theoretical predictions for hadron collider processes.

§1.3 QCD and hard scattering processes

A theoretical description of hadron collisions is complicated primarily by our limited knowledge of the strong force, which binds the elementary constituents of hadrons. Strong interactions are described by Quantum Chromodynamics (QCD), a non-Abelian gauge theory based on the SU(3) symmetry group. The QCD Lagrangian is not analytically solvable, making it extremely difficult to understand proton dynamics from first principles. A way to overcome these obstacles becomes manifest when we consider how hadrons collide at high energies [17]. Typically, they undergo either elastic scattering or diffractive dissociation: in the first case, they collide but remain intact; in the second, they disintegrate into a small number of hadrons. However, on rare occasions, a more interesting phenomenon can occur: the elementary partons that compose the hadrons can interact and exchange a large amount of momentum (~ 100 GeV). This is the case in so-called “hard scattering processes,” which are central to probing the electroweak scale, the Higgs boson, and potential new physics. Their importance is directly related to a key feature of the strong force: asymptotic freedom. The essence of this property is the weakening of the colour force at short distances [5]. In this high-energy regime, the interacting partons can be approximated as being nearly free, which permits a perturbative description of the strong interaction. The strength of these interactions is governed by the coupling constant α_S . Due to asymptotic freedom, α_S is on the order of 0.1 at energies relevant for contemporary colliders¹. This makes the strong force about ten times stronger than the electromagnetic interaction (whose coupling constant is $\alpha \sim 1/137$), yet sufficiently small to allow for the application of well-defined perturbative approximation methods.

§1.4 Hadronic cross-section and factorization theorem

A framework for describing these short-distance hard scattering processes is provided by the collinear factorization theorem [4]. Within this framework, colliding hadrons are treated as beams of partons, each carrying a certain fraction of the hadron’s total momentum. The probability of finding a parton with a specific energy fraction is encoded in the Parton Distribution Functions (PDFs). These functions are universal, meaning they are independent of the specific

¹This value is energy-dependent; $\alpha_S \sim 0.1$ is typical at energies around 100 GeV.

scattering process being studied. Consequently, PDFs can be measured in one set of experiments and then used to make predictions for many others [14]. The short-distance interaction of partons produces final states composed of Standard Model particles, such as leptons, gauge bosons, and additional QCD partons. The final-state partons, which are the direct products of the perturbative calculation, cannot be observed directly due to confinement². Instead, they evolve into collimated sprays of hadrons [10]. We interpret these partons as the seeds of hadronic jets and define the resulting sprays as jets themselves. At high energies, the properties of these jets are largely determined by the perturbative dynamics of their initiating parton and are only mildly affected by non-perturbative QCD effects.

The asymptotic freedom of QCD is what enables a perturbative description of the strong interaction. However, it is crucial to recognize that the precise mechanism allowing us to decouple the motion of partons from the proton's dynamics is the separation of energy scales involved. Interactions in the Standard Model typically probe energy scales on the order of $Q \sim 100 \text{ GeV} - 1 \text{ TeV}$, while the characteristic energy scale of hadronic structure and confinement is significantly lower, $\Lambda_{\text{QCD}} \sim 100 \text{ MeV}$.

The production cross section for final states involving QCD jets and other Standard Model particles in hard hadronic collisions is thus given by

$$d\sigma = \sum_{a,b} \int_0^1 dx_1 dx_2 f_a(x_1, \mu_F) f_b(x_2, \mu_F) d\hat{\sigma}_{a,b}(x_1, x_2, \mu_F, \mu_R; \mathcal{O}) \left(1 + \mathcal{O}\left(\frac{\Lambda_{\text{QCD}}}{Q}\right)^n \right), \quad n \geq 1 \quad (1.1)$$

where $f_{a,b}$ are the parton distribution functions mentioned above; $a, b \in \{g, d/\bar{d}, u/\bar{u}, s/\bar{s}, c/\bar{c}, b/\bar{b}\}$ represent the types of partons (gluons or quarks) inside the two colliding hadrons; x_1, x_2 are respectively the momentum fractions carried by partons a and b ; and \mathcal{O} is an infrared-finite observable.

The non-perturbative corrections in Eq. 1.1 are suppressed by powers of the ratio Λ_{QCD}/Q : in this case, Q represents the hard scale of the process, typically identified as the lowest transverse momentum (p_T) cut applied to final-state partons. For a typical cut of $Q \sim 20 \text{ GeV}$, this ratio is of order 10^{-2} . The exact power n of this suppression is process-dependent, and not always immediately evident, though for many applications the leading power is $n = 2$. This implies that the theoretical uncertainty from factorizing non-perturbative physics is of order $\mathcal{O}(10^{-4})$. Even when the leading power is only $n = 1$, the non-perturbative effects would be at the percent level ($\sim 10^{-2}$). This is comparable in size to the Next-to-Next-to-Leading Order (NNLO) QCD corrections for many processes. Therefore, a precise description of a process requires the inclusion of at least NNLO perturbative corrections before the inherent uncertainty from power corrections becomes significant.

This formalism establishes a clear distinction between the short-distance perturbative process and the long-distance non-perturbative physics. The boundary between these two regimes is defined by the factorization scale (μ_F). Processes with a momentum transfer $Q > \mu_F$ are treated as the hard scatter of point-like partons, calculable within perturbation theory. Physics at scales $Q < \mu_F$, which describes how the partons are bound within the proton, is incorporated into the non-perturbative Parton Distribution Functions (PDFs).

The other scale present in the factorized cross-section in Eq. 1.1 is the renormalization scale (μ_R). Its necessity arises because the calculation of partonic interactions in QCD using Feyn-

²Quark confinement is the phenomenon that prevents quarks and gluons from propagating as free particles over macroscopic distances.

man diagrams often results in ultraviolet (UV) divergences. These infinities do not indicate a fundamental error in the theory, but suggest a distinction between the bare parameters in the Lagrangian and physically observable quantities. The process of renormalization allows us to absorb these divergences into a redefinition of the Lagrangian's parameters, providing finite expressions for measurable quantities. The consequence of this procedure is that the coupling constant becomes a function of the energy scale, a phenomenon known as “running” [5]. The renormalization scale μ_R is the energy at which the coupling constant is defined, thereby encapsulating the quantum corrections of the theory.

Throughout this thesis, we set $\mu_F = \mu_R = \mu$. While a physical prediction must be independent of these arbitrary scales, cross-sections calculated within a fixed-order perturbative expansion exhibit a dependence on both the renormalization and factorization scales. Therefore, varying the scales around a central value and observing how the prediction changes provides a standard method for estimating the uncertainty associated with the truncation of the perturbative series.

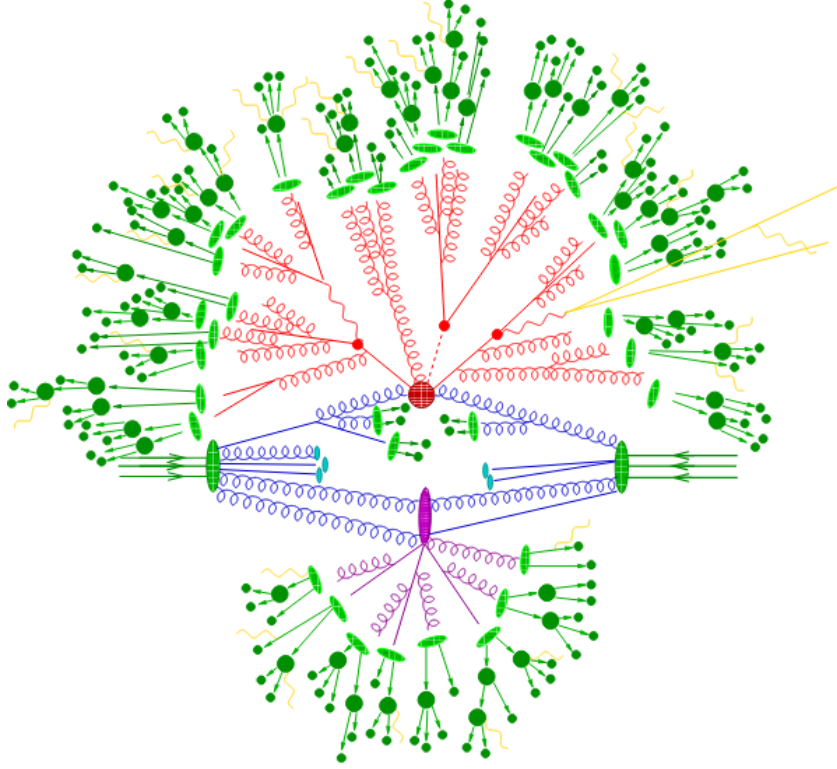


Figure 1.1: Sketch of an hard hadron-hadron collision at a collider like the LHC. The central red blob represents the hard interaction, a high-energy collision between two partons, calculable using perturbative QCD. The incoming and outgoing partons emit initial-state (blue) and final-state (red) radiation, producing many secondary particles. Softer underlying event activity (purple) arises from additional partonic interactions within the protons. A key feature is the hierarchy of energy scales: the hard process occurs at high energies ($Q > \Lambda_{\text{QCD}}$), while subsequent radiation and hadronization (green) take place at progressively lower scales, eventually transitioning to non-perturbative physics around Λ_{QCD} . Figure from [11].

Referring to Eq. 1.1, we can state that only the left-hand side represents a physically measurable quantity. The right-hand side, in contrast, consists of unobservable components: the parton

distribution functions (PDFs), which are extracted from experimental data, and the partonic cross-section $d\hat{\sigma}_{a,b}$, which is calculable within perturbation theory. It is therefore essential to understand how this latter quantity is computed.

§1.5 Partonic cross-section

We consider the inclusive³ production of N jets at a hadron collider, together with a color-neutral system X

$$pp \rightarrow X + N \text{ jets}. \quad (1.2)$$

As discussed above, we can use asymptotic freedom of QCD to expand the partonic cross section $d\hat{\sigma}_{a,b}$ in Eq. 1.1 in powers of the strong and the electroweak coupling constants, α_s and α ,

$$d\hat{\sigma}_{a,b} = d\hat{\sigma}_{a,b}^{(0,0)} + \alpha_s d\hat{\sigma}_{a,b}^{(1,0)} + \alpha_s^2 d\hat{\sigma}_{a,b}^{(2,0)} + \alpha_s^3 d\hat{\sigma}_{a,b}^{(3,0)} + \alpha d\hat{\sigma}_{a,b}^{(0,1)} + \alpha\alpha_s d\hat{\sigma}_{a,b}^{(1,1)} + \dots \quad (1.3)$$

Due to the different values of the coupling constants, at the same order they have a different impact on the final result: at NLO, QCD corrections account for approximately 10%, while EW account for 1%; at NNLO, QCD corrections account for 1%. Throughout this thesis, we will focus on the calculation of NLO QCD corrections.

The first term in this expansion $d\hat{\sigma}_{a,b}^{(0,0)} \equiv d\hat{\sigma}_{a,b}^{\text{LO}}$ is called Leading Order (LO), and it is defined as [20]

$$2s_{a,b} d\hat{\sigma}_{a,b}^{\text{LO}} = \mathcal{N} \int d\Phi (2\pi)^4 d\text{Lips}_X \delta^{(4)}(p_{\mathcal{H}_f} + p_X - p_a - p_b) |\mathcal{M}_0(p_a, p_b; p_{\mathcal{H}_f}, p_X)|^2 \mathcal{O}(p_{\mathcal{H}}, p_X). \quad (1.4)$$

With \mathcal{H}_f , we denote the list of final-state resolved particles, and $p_{\mathcal{H}_f}$ is their momentum, while p_X denotes the momentum of the color-singlet in the hard process. \mathcal{N} is a normalization factor: it takes into account color and spin averages as well as symmetry factors. With $s_{a,b}$, we express the partonic center-of-mass energy squared: $s = (p_a + p_b)^2 = 2p_a \cdot p_b$, considering massless partons. The matrix element for the considered process is denoted by \mathcal{M}_0 , and \mathcal{O} represents an infrared-safe observable that ensures the final state contains at least N resolved jets. This latter feature is crucial because infrared dynamics are non-perturbative and, consequently, cannot be described by an expansion in α_s . Finally, $d\text{Lips}_X$ is the Lorentz-invariant phase space for the colorless particle X , including the momentum-conserving delta function, and $d\Phi$ is the Lorentz-invariant phase space for the final-state particles.

$$d\Phi = \prod_{i \in \mathcal{H}_f} [dp_i], \quad [dp_i] = \frac{d^3 p_i}{(2\pi)^3 2E_i}, \quad (1.5)$$

where $[dp_i]$ is the phase-space element of a final-state parton i . Moreover, in Eq. 1.4, summation over spins and colors of final-state partons, and averaging over spins and colors of initial-state partons are assumed.

For notational compactness, we introduce the function F_{LM}^{ab} , defined as in Section 2 of [19]

$$F_{\text{LM}}^{ab} = d\text{Lips}_X |\mathcal{M}_0|^2 \mathcal{O}. \quad (1.6)$$

³The inclusive cross-section counts every collision event that creates a specific particle, whether it appears alone, with jets, or with any other additional radiation. It gives the total production rate, ignoring the details of what else is produced alongside it.

We denote the integration over the final-state phase space of Eq. 1.6 with the angular brackets $\langle \dots \rangle$, and obtain exactly Eq. 1.4

$$2s_{a,b} d\hat{\sigma}_{a,b}^{\text{LO}} = \langle F_{\text{LM}}^{ab}[\dots] \rangle. \quad (1.7)$$

At Leading Order (LO), calculations are performed directly. The tree-level matrix elements can be computed easily using helicity techniques and colour-subamplitude decompositions [3], and are then integrated, either numerically or analytically.

The strong coupling constant in hard scattering processes is small enough to allow for a perturbative description, but not enough to make higher-order corrections entirely negligible. Therefore, in order to claim high precision, we also need to compute QCD corrections. According to the factorization theorem, the computed partonic cross-section should be insensitive to long-distance effects, which are absorbed into the parton distribution functions. The QCD corrections instead account for short-distance, high-energy effects at higher orders in the coupling constant. The NLO correction $d\hat{\sigma}_{a,b}^{(1,0)} \equiv d\hat{\sigma}_{a,b}^{\text{NLO}}$ to a partonic cross section consists of three terms: the one-loop (virtual) contribution, the real emission contribution, and the contribution related to parton distribution functions

$$d\hat{\sigma}_{a,b}^{\text{NLO}} = d\hat{\sigma}_{a,b}^{\text{V}} + d\hat{\sigma}_{a,b}^{\text{R}} + d\hat{\sigma}_{a,b}^{\text{pdf}}. \quad (1.8)$$

The last term, $d\hat{\sigma}_{a,b}^{\text{pdf}}$, is generated by the renormalization of the PDFs at LO, and its expression is known [7]. The other terms, $d\hat{\sigma}_{a,b}^{\text{V}}$ and $d\hat{\sigma}_{a,b}^{\text{R}}$, are related to either the emission of an additional leg in the Feynman diagram, i.e., an extra parton in the final state (real correction), or to the emission and reabsorption of a parton through a loop (virtual correction).

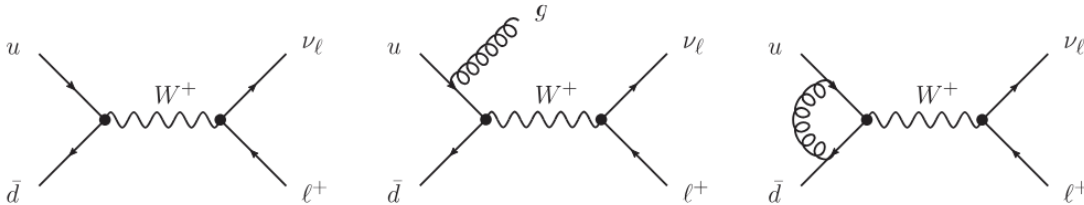


Figure 1.2: Feynman diagrams for W boson production at hadron colliders. The diagram on the left corresponds to the leading-order (LO) calculation of the total cross-section. The diagrams shown in the middle and on the right represent the real and virtual corrections, respectively, which together constitute the next-to-leading-order (NLO) contributions to the total cross-section. Figure from [13]

It is important to emphasize that while the concepts of “real” and “virtual” radiation are physically well-defined, their separate contributions to the partonic cross-section, $d\hat{\sigma}_{a,b}$, are not physically observable. The division into real and virtual terms is therefore a computational tool, introduced to organize the calculation and manage the various contributions more effectively. The treatment of these terms is non-trivial, as they exhibit divergences in specific energy regimes. The virtual contributions, for instance, contain ultraviolet (UV) singularities. These are removed through the process of renormalization⁴, a procedure that ensures physical observables, when expressed in terms of appropriately defined renormalized parameters, become

⁴Throughout this thesis, we work with UV-renormalized matrix elements.

insensitive to the high-energy UV region.

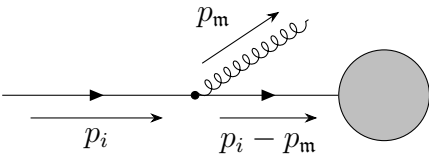
Furthermore, the low-momentum (soft) and small-angle (collinear) kinematic regions produce singularities in both the real and virtual contributions. These infrared (IR) singularities are not independent: the real and virtual corrections are fundamentally linked by their infrared behavior. The divergence of scattering amplitudes in the soft or collinear limit means these kinematic configurations must be carefully handled to obtain meaningful results. Consequently, a precise procedure for removing these divergences is of the highest importance for calculating finite cross-sections.

§1.6 Infrared poles and their cancellation

In order to deal with IR divergences, it is convenient to employ dimensional regularization [2]. This technique involves the analytical continuation of momentum space from 4 to $d = 4 - 2\epsilon$ dimensions, where $\epsilon \in \mathbb{C}$ and $\text{Re}(\epsilon) < 0$. In this framework, divergences appear as poles in $1/\epsilon$ in the complex dimensional plane.

The virtual corrections $d\hat{\sigma}_{a,b}^V$ contain explicit infrared and collinear poles, which are independent of the details of the hard matrix element [7]. In contrast, the real emission contribution $d\hat{\sigma}_{a,b}^R$ contains kinematic singularities that only become explicit $1/\epsilon$ poles upon integration over the phase space of the additional final-state parton. However, we must avoid a naive integration over the entire radiation phase space, as it would render the cross section inclusive rather than differential, discarding all information on the kinematics of the radiated parton. This information is often crucial since jet properties provide essential data for defining experimental signatures.

QCD amplitudes for real emission processes become singular in kinematic limits where the gluon becomes soft (low energy) or any parton (quark, antiquark, gluon) is emitted collinearly to another parton. In these limits, the propagator of the emitted particle approaches its on-shell condition, leading to divergent behavior. To show this, consider a diagram that describes an emission of a gluon (\mathbf{m}) off an external incoming quark (i) line



$$\sim \frac{1}{(p_i - p_m)^2} = \frac{1}{2E_i E_m (1 - \cos \theta_{im})} \xrightarrow{E_m, \theta_{im} \rightarrow 0} \infty.$$

For massless partons ($|\mathbf{p}_i| = E_i$, $|\mathbf{p}_i|^2 = 0$), the amplitude exhibits a clear divergence in both the soft and collinear limits, that is when E_m or $\theta_{im} \rightarrow 0$.

It is important to consider the origin of these infinities. The presence of divergences is, in fact, a manifestation of long-distance effects: they signal that non-perturbative contributions are entering our perturbative calculation. This could be a problem, as we lack methods to treat non-perturbative QCD effects from first principles [14]. Fortunately, once the $1/\epsilon$ poles are extracted from both the virtual and real corrections, their sum is guaranteed to be free of infrared divergences due to the Bloch-Nordsieck [1] and Kinoshita-Lee-Nauenberg theorems. Therefore, perturbative QCD corrections remain insensitive to the details of infrared physics. However, achieving the cancellation of the $1/\epsilon$ poles by simply summing the real and virtual corrections is not straightforward. This complication arises because the virtual corrections are defined in an n -particle phase space, whereas the real corrections inhabit an $(n + 1)$ -particle

phase space. We might think that this problem could be avoided by integrating over the phase space. However, this approach would only yield a total cross-section, not a differential one, as stated above. This mismatch in the dimensionality of the integration domains, combined with the need to extract the implicit $1/\epsilon$ poles from the real-emission contributions, without performing the full integration, is precisely why dedicated subtraction schemes are required. Over time, various methods have been developed to perform fully differential QCD computations for hadron collider processes, both at NLO and NNLO. Among the existing methods, in this thesis we will focus on the Nested Soft-Collinear (NSC) Subtraction Scheme [12], which will be detailed in Chapter 2. The numerical stability and computational efficiency of this method can, however, be further improved. A step forward in this direction will be presented in Chapter 3; this represents the original contribution of this thesis.

NLO QCD corrections in the NSC Subtraction Scheme

The singular limits of NLO QCD amplitudes, as well as the methods for using them to compute NLO QCD cross sections, are well established [6, 7]. Furthermore, all the singular limits of QCD amplitudes necessary for calculating NNLO QCD corrections have been known for approximately two decades. However, it took significant time to determine how to combine these NNLO limits with the ideas from the NLO Frixione-Kunszt-Signer (FKS) subtraction scheme [6] to construct a valid subtraction method for NNLO computations. Among the numerous proposed methods, the Nested Soft-Collinear Subtraction Scheme (NSC SS), introduced in [12], is particularly attractive, for reasons that will become clear throughout the following discussion.

This chapter provides an overview of the main results achieved. Since the objective of this thesis is to implement parameters that allow for greater control over the integrated phase-space region, and since these parameters appear only in the real corrections, we will focus exclusively on the latter. Moreover, the divergent parts of the virtual corrections can be isolated using Catani's representation of renormalized one-loop scattering amplitudes [8]. Although these methods have been implemented up to NNLO, this thesis will focus on the NLO case, as its relative simplicity offers a clearer understanding of how to implement the parameters.

§2.1 Properties of Soft and Collinear partons

The desired method necessitates the isolation of singularities in the real corrections without integrating over the momenta of any of the final-state particles, in order to keep the kinematics of all the final-state particles intact. There are two key insights that allow us to overcome this obstacle. The first one is related to the behaviour of NLO QCD amplitudes at soft and collinear limits.

For a generic QCD amplitude \mathcal{M} involving n partons with four-momenta p_1, p_2, \dots, p_n and an additional soft gluon with vanishing four-momentum p_m , the squared amplitude factorizes into (i) the squared amplitude for the hard process without the gluon and (ii) an eikonal factor that depends only on the color charges and momenta of the hard partons and the momentum of the soft gluon (p_m) [9]

$$\lim_{E_m \rightarrow 0} |\mathcal{M}(p_1, p_2, \dots, p_n; p_m)|^2 = -4\pi\alpha_s \mu^{2\epsilon} \sum_{i,j=1}^n \mathcal{S}_{ij}(p_m) \vec{T}_i \cdot \vec{T}_j |\mathcal{M}_0(p_1, p_2, \dots, p_n)|^2, \quad (2.1)$$

where the *general eikonal factor* is

$$\mathcal{S}_{ij}(p_{\mathbf{m}}) = \frac{p_i \cdot p_j}{(p_i \cdot p_{\mathbf{m}})(p_j \cdot p_{\mathbf{m}})}, \quad (2.2)$$

and the square of the color charges are $\vec{T}_i^2 = C_F$ if i is a quark or an anti-quark, and $\vec{T}_i^2 = C_A$ if i is a gluon.

Whereas, in the collinear limit, i.e., the limit where a gluon is emitted parallel to a quark, the amplitude-squared factorizes into (i) a *splitting function*, which describes the probability for the quark to radiate the gluon collinearly at a given energy, and (ii) the squared hard amplitude, which now depends on the resulting quark momentum after the emission

$$\lim_{\theta_{i\mathbf{m}} \rightarrow 0} |\mathcal{M}(p_1, \dots, p_n; p_{\mathbf{m}})|^2 \sim P_{f_{[i\mathbf{m}]f_i}} |\mathcal{M}_0(p_1, \dots, p_i + p_{\mathbf{m}}, \dots, p_n)|^2. \quad (2.3)$$

The unresolved parton \mathbf{m} could also be a quark or an antiquark. However, the emission of a soft quark leads to a convergent integral; consequently, no divergences are associated with soft quark or antiquark emissions. Divergences do arise in the collinear limit, but, as in the gluon case, the amplitude factorizes into a hard process involving a parton with rescaled momentum and a corresponding splitting function.

Equation 2.1 shows that the dependence on $p_{\mathbf{m}}$ lies only in the eikonal function, while \mathcal{M}_0 is independent of $p_{\mathbf{m}}$. Instead, Equation 2.3 shows that the dependence on the unresolved momentum is absorbed into the rescaled momentum of parton i within the hard matrix element \mathcal{M}_0 , while the singular behavior is captured by the splitting function. These remarks will be fundamental to construct properly a subtraction method.

The second important insight is that, in singular kinematic regions, real emissions are always unresolved, meaning they lack a distinct experimental signature. Consequently, we can safely integrate over the singular regions of their phase space without losing any physically observable information.

§2.2 Why a subtraction method

Let us first present the core idea of the subtraction formalism. We consider the integral

$$I = \int_0^1 dx \frac{1}{x^{1+\epsilon}} F(x), \quad (2.4)$$

where $F(x)$ is an arbitrary function regular at $x = 0$. The integrand diverges at the lower limit, and this singularity is regulated by the parameter ϵ , which ultimately produces a $1/\epsilon$ pole upon integration. We want to isolate this pole analitically, and define the integral in such a way that the limit $\epsilon \rightarrow 0$ can be taken safely. To achieve this, we write $F(x) = [F(x) - F(0)] + F(0)$

$$I = \int_0^1 dx \frac{1}{x^{1+\epsilon}} [F(x) - F(0)] + F(0) \int_0^1 dx \frac{1}{x^{1+\epsilon}}, \quad (2.5)$$

and, performing the integration in the second term, we get

$$I = \int_0^1 \frac{dx}{x} [F(x) - F(0)] - \frac{1}{\epsilon} F(0) + \mathcal{O}(\epsilon). \quad (2.6)$$

This equation demonstrates that we have successfully isolated the $1/\epsilon$ pole in I and regulated the integrand. As a result, the $\epsilon \rightarrow 0$ limit can now be taken safely, leaving an integral that is regular at $x = 0$ and can be evaluated numerically.

Now, suppose we have a function \mathcal{S} that reproduces the leading singular behaviour of F_{LM}^{ab} (defined in Eq. 1.6) in all soft and collinear limits, and that can be integrated in the d -dimensional phase space of the unresolved parton \mathbf{m} . We can then write the real-emission cross section as

$$2s_{a,b} d\hat{\sigma}_{a,b}^{\text{R}} = \int [dp_{\mathbf{m}}] F_{\text{LM}}^{ab} = \int [dp_{\mathbf{m}}] (F_{\text{LM}}^{ab} - \mathcal{S}) + \int [dp_{\mathbf{m}}] \mathcal{S} \quad (2.7)$$

where $[dp_{\mathbf{m}}]$ is the d -dimensional phase-space measure for the emitted gluon, now also incorporating the theta function to enforce energy conservation

$$[dp_{\mathbf{m}}] = \frac{d^{d-1}p_{\mathbf{m}}}{(2\pi)^{d-1}2E_{\mathbf{m}}} \theta(E_{\text{max}} - E_{\mathbf{m}}), \quad (2.8)$$

and E_{max} is an arbitrary energy scale that must be at least as large as the maximum energy allowed by the momentum-conserving δ -functions in Eq. 1.4.

On the right-hand side of Eq. 2.7, the first term is integrable in four-dimensional phase space, since the leading singular behaviour of F_{LM}^{ab} is removed by the subtraction term \mathcal{S} . As this integration is performed numerically using Monte Carlo (MC) methods, it is clear that restricting the integration region to the minimal necessary volume is crucial for improving the efficiency of the computation.

The second term involves only the unresolved parton \mathbf{m} , making it possible to integrate over its phase space without affecting the jet observables. Furthermore, as showed in Eq. 2.6, this integration enables the extraction of $1/\epsilon$ poles, which describe the singular behaviour of \mathcal{S} and, consequently, of the amplitude itself. Moreover, it resolves the problem of the dimensional mismatch between the integration domains of the virtual and real corrections. Thus, the cancellation of the poles with those arising from the virtual contributions becomes possible.

§2.3 Soft and Collinear operators

Different subtraction schemes are characterized by different forms for \mathcal{S} , or, equivalently, $F(0)$. The FKS subtraction scheme, which constitutes the basis for the NSC method, constructs \mathcal{S} directly from the soft and collinear limits. The efficacy of this approach becomes clear if we consider the behaviour of the amplitudes in these limits, as detailed in Section 2.1: in both the soft and collinear cases, the amplitude squared factorizes into a lower-multiplicity function F_{LM}^{ab} , which is independent of the unresolved parton \mathbf{m} , and a singular term, whose integration over the phase space of parton \mathbf{m} gives the explicit pole. Therefore, we introduce two operators that perform soft and collinear projections

$$S_i A = \lim_{E_i \rightarrow 0} A, \quad C_{ij} A = \lim_{\rho_{ij} \rightarrow 0} A, \quad (2.9)$$

where $\rho_{ij} = 1 - \vec{n}_i \cdot \vec{n}_j = 1 - \cos \theta_{ij}$, with \vec{n}_i a unit vector that describes the direction of the momentum of the i -th particle in $(d-1)$ -dimensional space, and θ_{ij} the angle between partons i and j . These operators apply to all terms that follow them.

Thus, we identify \mathcal{S} as the action of the soft and/or collinear operators on F_{LM}^{ab} . As these operators capture the leading asymptotic behaviour of the product of the matrix element squared,

the observable, and the phase space – namely, the definition of F_{LM}^{ab} in Eq. 1.6, if this quantity is, instead, integrable, the operator acts as an annihilator (e.g., $S_q = S_{\bar{q}} = 0$).

The singularities are isolated and extracted sequentially in a nested manner: first, the soft singularities are removed, followed by the collinear and soft-collinear ones, using an identity operator constructed as follows:

$$\mathbb{1} = S_{\mathbf{m}} + \sum_{i \in \mathcal{H}} \bar{S}_{\mathbf{m}} C_{i\mathbf{m}} + \sum_{i \in \mathcal{H}} \bar{S}_{\mathbf{m}} \bar{C}_{i\mathbf{m}} \omega^{\mathbf{m}i}, \quad (2.10)$$

where $\bar{S}_{\mathbf{m}} = \mathbb{1} - S_{\mathbf{m}}$, $\bar{C}_{\mathbf{m}} = \mathbb{1} - C_{\mathbf{m}}$, $\mathcal{H} = \mathcal{H}_f \cup \{a, b\}$, and $\omega^{\mathbf{m}i}$ are partition functions that allow for treating one collinear singularity at a time by splitting the phase space, and satisfy the following equation

$$\sum_{i \in \mathcal{H}} \omega^{\mathbf{m}i} = 1. \quad (2.11)$$

It is also convenient to partition the phase space in such a way that some partons are classified as “hard” and thus cannot give rise to infrared singularities. For this purpose, we define so-called “damping factors” (see Appendix A.2), which can be used to construct a partition of unity

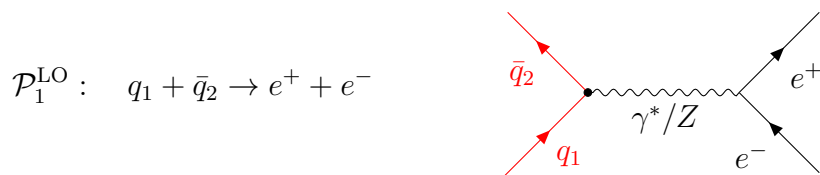
$$\sum_{i \in \mathcal{H}_f} \Delta^{(i)} = 1. \quad (2.12)$$

The damping factor $\Delta^{(i)}$ acts as an annihilator, vanishing when any parton other than i becomes unresolved.

§2.4 Modularity of the scheme

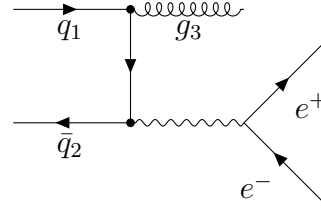
One of the most interesting features of the NSC subtraction scheme is its modular structure: the subtractions for a generic process, no matter how complicated, are built from a relatively small set of basic ingredients. Indeed, the soft contributions are straightforward to compute, while, for the nested-soft-collinear ones, we only need to consider pairs of partons. This leads to three possible cases: both partons are initial state, both are final state, or one is initial and one is final. These three possibilities have been studied in [15], [16], and [18], respectively. Therefore, in order to better understand the workings of the NSC subtraction scheme with all its subtleties, the following sections will present a general treatment, while making explicit reference to specific examples, namely the processes discussed in [15] and [16].

Ref. [15] provides the analytic formulas for the production of a generic color-singlet final state V at a hadron collider, i.e., $q_1 \bar{q}_2 \rightarrow V$ (which we will call $\mathcal{P}_1^{\text{LO}}$), such as the Drell-Yan process, illustrated in the following diagram



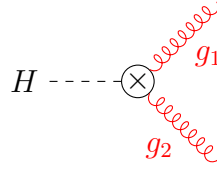
The real emission contribution refers to the process $\mathcal{P}_1^{\text{NLO}} : q_1 \bar{q}_2 \rightarrow V + g_3$, that, in the case of Drell-Yan, can be represented as

$$\mathcal{P}_1^{\text{NLO}} : \quad q_1 + \bar{q}_2 \rightarrow e^+ + e^- + g_3$$



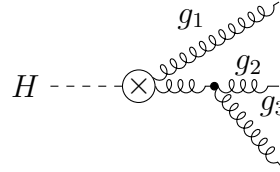
Instead, Ref. [16] considers the decay of a color-singlet particle Q into quarks and gluons, and, in particular, the process $\mathcal{P}_2^{\text{LO}} : Q \rightarrow f_i f_j + X$, where $\{f_i, f_j\}$ can be either $\{g, g\}$ or $\{q, \bar{q}\}$. We will focus on the discussion of the decay to a gg final state since its singularity structure is more complex: once the corrections for $Q \rightarrow gg$ are understood, the corrections for $Q \rightarrow q\bar{q}$ are easily derived. This process, if for instance Q is the Higgs boson, is represented by the following diagram

$$\mathcal{P}_2^{\text{LO}} : H \rightarrow g_1 + g_2$$



where \otimes denotes the effective local vertex, which encapsulates the top-quark loop contribution. NLO QCD contributions come from the following process

$$\mathcal{P}_2^{\text{NLO}} : H \rightarrow g_1 + g_2 + g_3$$



Our goal is to present the explicit expression for the real-emission contributions in a form similar to that of Catani's $I_1(\epsilon)$ function defined in Ref.[8], by introducing two operators, I_S and $I_C(\epsilon)$, which parametrize the poles arising from the soft and collinear limits, respectively. The corrections will then be given by the product of these functions with the leading-order kinematics, so that the sum

$$I_T(\epsilon) = I_V(\epsilon) + I_S(\epsilon) + I_C(\epsilon), \quad (2.13)$$

is finite as $\epsilon \rightarrow 0$, where $I_V(\epsilon)$ is related to $I_1(\epsilon)$.

§2.5 Soft limit

Let \mathbf{m} be the index that characterizes the unresolved parton. To define the expression of the last term on the right-hand side of Eq. 2.7 in the soft limit, it is necessary to integrate over the phase space of the parton \mathbf{m} in Eq. 2.1, i.e., the result of the action of the soft operator on the squared matrix element. In this case, we can express Eq. 2.1 as

$$\langle \Delta^{(\mathbf{m})} F_{\text{LM}}(\mathbf{m}) \rangle = \langle S_{(\mathbf{m})} F_{\text{LM}}(\mathbf{m}) \rangle + \langle \bar{S}_{(\mathbf{m})} F_{\text{LM}}(\mathbf{m}) \rangle, \quad (2.14)$$

where the soft operator acting on the splitting function yields $S_m \Delta^m = 1$. Before performing the integration, we note that it is convenient to express the phase-space measure $[dp_m]$ from Eq. 2.8 in hyperspherical coordinates. For massless partons (where $|p_m| = E_m$), this measure becomes

$$[dp_m] = \frac{E_m^{d-3} dE_m d\Omega_{d-1}}{2(2\pi)^{d-1}} \theta(E_{\max} - E_m), \quad (2.15)$$

where $d\Omega_{d-1}$ is the $(d-1)$ -dimensional solid-angle element. Using the bare QCD coupling $g_{s,b}^2 = 4\pi\alpha_s$ and considering N_p partons at Leading Order, we obtain

$$\langle S_m F_{\text{LM}}(\mathbf{m}) \rangle = \int dE_m E_m^{d-5} \theta(E_{\max} - E_m) \int \frac{d\Omega_{d-1}}{2(2\pi)^{d-1}} (-g_{s,b}^2) \sum_{(i \neq j)}^{N_p} \frac{\rho_{ij}}{\rho_{im} \rho_{jm}} (\vec{T}_i \cdot \vec{T}_j) F_{\text{LM}}, \quad (2.16)$$

where we do not list all the partons involved in the process as arguments of F_{LM} , but we only specify if it depends on the unresolved parton \mathbf{m} . Recall that $\rho_{ij} = 1 - \cos \theta_{ij}$, so that the dot product is $p_i \cdot p_j = E_i E_j \rho_{ij}$. We now evaluate the integrals using dimensional regularization in $d = 4 - 2\epsilon$ dimensions. The energy integral yields a simple pole in ϵ

$$\int_0^{E_{\max}} \frac{dE_m}{E_m^{1+2\epsilon}} = -\frac{1}{2\epsilon} E_{\max}^{-2\epsilon}. \quad (2.17)$$

Regarding the angular integral, we utilize a standard result, given for instance in Appendix G.2 of [18]

$$\int \frac{d\Omega_{d-1}}{2(2\pi)^{d-1}} \frac{\rho_{ij}}{\rho_{ik} \rho_{jk}} = -\frac{2^{1-2\epsilon}}{\epsilon} \left[\frac{1}{8\pi^2} \frac{(4\pi)^\epsilon}{\Gamma(1-\epsilon)} \right] \eta_{ij}^{-\epsilon} K_{ij}, \quad (2.18)$$

with

$$K_{ij} = \left[\frac{\Gamma^2(1-\epsilon)}{\Gamma(1-2\epsilon)} \right] \eta_{ij}^{1+\epsilon} {}_2F_1(1, 1; 1-\epsilon; 1-\eta_{ij}), \quad (2.19)$$

where $\eta_{ij} = \rho_{ij}/2$, and ${}_2F_1$ denotes the Gauss hypergeometric function. Combining these results, we get

$$\langle S_m F_{\text{LM}}(\mathbf{m}) \rangle = -\frac{[\alpha_s]}{\epsilon^2} \left(\frac{2E_{\max}}{\mu} \right)^{-2\epsilon} \sum_{(ij)}^{N_p} \eta_{ij}^{-\epsilon} K_{ij} (\vec{T}_i \cdot \vec{T}_j) F_{\text{LM}}, \quad (2.20)$$

where we have introduced the short-hand notation

$$[\alpha_s] = \frac{\alpha_s(\mu)}{2\pi} \frac{e^{\epsilon\gamma_E}}{\Gamma(1-\epsilon)}, \quad (2.21)$$

with $\alpha_s(\mu)$ the running coupling constant, and γ_E the Euler-Mascheroni constant. Therefore, the integrated soft-counterterm reads

$$\langle S_m F_{\text{LM}}(\mathbf{m}) \rangle = [\alpha_s] \langle I_S(\epsilon) \cdot F_{\text{LM}} \rangle, \quad (2.22)$$

with

$$I_S(\epsilon) = -\frac{(2E_{\max}/\mu)^{-2\epsilon}}{\epsilon^2} \sum_{(ij)}^{N_p} \eta_{ij}^{-\epsilon} K_{ij} (\vec{T}_i \cdot \vec{T}_j). \quad (2.23)$$

To better understand this result, we now consider its expression in the specific cases mentioned above. For process $\mathcal{P}_1^{\text{NLO}}$, the only parton that can become unresolved is the gluon g_3 . Therefore, the dot product $\vec{T}_i \cdot \vec{T}_j$ refers to quarks q_1 and q_2 , and evaluates to $\vec{T}_q^2 = C_F$ (see Eq. A.1). Moreover, in this case we have a significant simplification: we work in the frame where the partons q_1 and q_2 collide head-on, meaning that $\theta_{12} = \pi$, and $\eta_{12} = \rho_{12}/2 = 1$. Thus, Eq. 2.20 becomes

$$\langle S_3 F_{\text{LM}}(1, 2, 3) \rangle = [\alpha_s] \frac{2C_F(2E_{\text{max}}/\mu)^{-2\epsilon}}{\epsilon^2} \frac{\Gamma^2(1-\epsilon)}{\Gamma(1-2\epsilon)} F_{\text{LM}}(1, 2), \quad (2.24)$$

where $F_{\text{LM}}(\dots)$ denotes the corresponding parton-level matrix element squared, as defined in Eq. 1.6, and now has the arguments specifying all the partons involved in the process.

In the case of $\mathcal{P}_2^{\text{NLO}}$, each of the three gluons involved in the process can become unresolved. However, due to the symmetry of the matrix element and the phase space, the three possibilities yield analogous results. We therefore consider, for example, the case where $\mathbf{m} = 3$, meaning that gluons g_1 and g_2 are resolved, and only gluon g_3 can become unresolved. In this case, $i = 1$ and $j = 2$ (and vice versa); therefore, the dot product $\vec{T}_i \cdot \vec{T}_j$ refers to gluons and is equal to $\vec{T}_g^2 = C_A$ (see Eq. A.1). The calculation is analogous to the one performed in the general case, as it involves integrating the eikonal factor in Eq. 2.2 over the phase space of the unresolved parton. If we expand the function K_{12} defined in Eq. 2.19 in ϵ , we obtain the following result

$$\langle S_3 F_{\text{LM}}(1, 2, 3) \rangle = [\alpha_s] \frac{1}{3} \frac{2C_A(m_H/\mu)^{-2\epsilon}}{\epsilon^2} \eta_{12}^{-\epsilon} [1 + \epsilon^2(\text{Li}_2(1 - \eta_{12}) - \zeta_2) + \mathcal{O}(\epsilon^2)] F_{\text{LM}}(1, 2), \quad (2.25)$$

where m_H is the mass of the Higgs boson, and $1/3$ is a symmetry factor.

§2.6 Collinear and Soft-Collinear limits

We observe that the last term in Eq. 2.22 is regulated in the soft limit, but it still contains collinear divergences. To isolate and remove them, we rewrite the expression as

$$\langle \Delta^{(\mathbf{m})} F_{\text{LM}}(\mathbf{m}) \rangle = \langle S_{(\mathbf{m})} F_{\text{LM}}(\mathbf{m}) \rangle + \sum_{i=1}^{N_p} \langle \bar{S}_{(\mathbf{m})} C_{i\mathbf{m}} \Delta^{(\mathbf{m})} F_{\text{LM}}(\mathbf{m}) \rangle + \langle \bar{S}_{(\mathbf{m})} \bar{C}_{i\mathbf{m}} \Delta^{(\mathbf{m})} \omega^{\mathbf{m}i} F_{\text{LM}}(\mathbf{m}) \rangle, \quad (2.26)$$

where the final term on the right-hand side is completely finite and can be integrated in four dimensions.

The collinear limits are a local phenomenon. Their analysis requires only the identification of the partons involved in the splitting: specifically, whether they are quarks or gluons and if they are in the initial or final state. The remaining details of the hard scattering process are irrelevant. When a final-state parton \mathbf{m} becomes collinear with another final-state parton i , the process is described by $[i\mathbf{m}]^* \rightarrow i(z) + \mathbf{m}(\bar{z})$. In this splitting, the variable $z = 1 - E_{\mathbf{m}}/E_{[i\mathbf{m}]}$ defines the energy fraction carried by parton i , while parton \mathbf{m} carries the complementary fraction $1 - z$. Conversely, when an outgoing parton \mathbf{m} becomes collinear with an incoming parton i , they are clustered into a parton $[i\mathbf{m}]$. This process is described as $i \rightarrow [i\mathbf{m}]^* + \mathbf{m}$, with $z = 1 - E_{\mathbf{m}}/E_i$. The specific identity of the parton $[i\mathbf{m}]$ that enters the hard process depends on this configuration, leading to different splitting functions in Eq. 2.3: a gluon clustered with any type of parton

preserves the latter's flavours, while a quark clustered with an antiquark gives a gluon. It is precisely this property that ensures the modularity of the NSC scheme, as previously discussed.

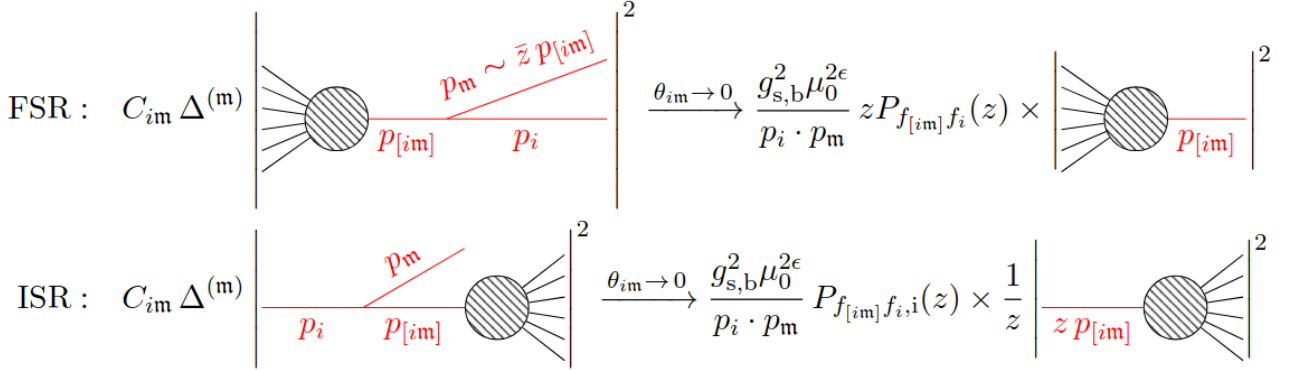


Figure 2.1: Graphical representation of the convention used for collinear factorization. The upper diagram illustrates the final-state splitting process, whereas the lower diagram represents the initial-state splitting process. We observe that for Final-State Radiation (FSR), the action of the operator C_{im} on $\Delta^{(m)}$ introduces an additional factor of z , a feature that is absent in Initial-State Radiation (ISR). Figure from [21].

§2.6.1 Initial state

We consider the situation where a gluon \mathbf{m} in the final state becomes collinear to a quark a in the initial state. This could happen, for instance, in the case of process $\mathcal{P}_1^{\text{NLO}}$. The squared matrix element, which is used to define the function F_{LM} , has a dependence on the energy fraction variable $z = 1 - E_{\mathbf{m}}/E_a$. As a direct consequence of this dependence, the integral over the collinear gluon's energy cannot be performed. Nevertheless, we can still carry out the angular integration over the relative angle between the emitted gluon \mathbf{m} and the incoming parton a .

We begin by examining how the cross section factorizes upon the application of the collinear operator

$$C_{am} \Delta^{(m)} F_{\text{LM}} = \frac{g_{s,b}^2}{p_a \cdot p_m} \frac{P_{qq}(z)}{z} F_{\text{LM}}(z \cdot a_q), \quad (2.27)$$

where $z \cdot a_q$ denotes a quark whose momentum is the product of z and the momentum of the incoming quark a . This relationship is the fundamental reason we cannot integrate over $E_{\mathbf{m}}$. The corresponding splitting function for this limit is

$$P_{qq}(z) = C_F \left[\frac{1+z^2}{1-z} - \epsilon(1-z) \right]. \quad (2.28)$$

If, instead, both the soft and collinear operators are applied, one obtains

$$C_{am} S_m F_{\text{LM}}(a_q, \mathbf{m}) = \lim_{z \rightarrow 1} C_{am} F_{\text{LM}}(a_q, \mathbf{m}) = \frac{g_{s,b}^2}{p_a \cdot p_m} \frac{2C_F}{1-z} F_{\text{LM}}(a_q). \quad (2.29)$$

Also in this case, it is convenient to perform the integration in hyperspherical coordinates. Furthermore, it is useful to implement a change of variables by parametrizing the gluon energy

as $E_{\mathbf{m}} = (1 - z)E_a$, which implies that the measure transforms as $dE_{\mathbf{m}} = -E_a dz$. Therefore, Eq. 2.15 becomes

$$[dp_{\mathbf{m}}] = \frac{E_a^{d-2} (1 - z)^{d-3} dz d\Omega^{d-1}}{2 (2\pi)^{d-1}} \theta(z - z_{\min}), \quad (2.30)$$

where $z_{\min} = 1 - E_{\max}/E_a$, and $d = 4 - 2\epsilon$. We also note that $p_a \cdot p_{\mathbf{m}} = E_a E_{\mathbf{m}} \rho_{am} = (1 - z)E_a^2 \rho_{am}$. We can therefore proceed with the integration. For the moment, we will only explicitly perform the phase space integration for partons a and \mathbf{m} , which are directly involved in the change of variables

$$\begin{aligned} & \int [dp_{\mathbf{m}}] \int [dp_a] C_{am} \bar{S}_{\mathbf{m}} F_{\text{LM}}(a_q, \mathbf{m}) = \\ & = g_{s,b}^2 \int [dp_a] \int \frac{d\Omega^{d-1}}{2(2\pi)^{d-1}} E_a^{-2\epsilon} \int_{z_{\min}}^1 dz (1 - z)^{-2\epsilon} \frac{1}{\rho_{am}} \left[\frac{P_{qq}(z)}{z} F_{\text{LM}}(z \cdot a_q) - \frac{2C_F}{1 - z} F_{\text{LM}}(a_q) \right]. \end{aligned} \quad (2.31)$$

Now we solve the angular integral using the following equation, Eq. G.5 in [18]

$$\int \frac{d\Omega^{d-1}}{2(2\pi)^{d-1}} \frac{1}{\rho_{am}} = -\frac{2^{-2\epsilon}}{\epsilon} \left[\frac{(4\pi)^\epsilon}{8\pi^2 \Gamma(1 - \epsilon)} \right] \left[\frac{\Gamma^2(1 - \epsilon)}{\Gamma(1 - 2\epsilon)} \right]. \quad (2.32)$$

Moreover, we use the shorthand notation $[\alpha_s]$ in Eq. A.3. Thus, Eq. 2.31 becomes

$$\begin{aligned} & \int [dp_{\mathbf{m}}] \int [dp_a] C_{am} \bar{S}_{\mathbf{m}} \Delta^{(\mathbf{m})} F_{\text{LM}}(a_q, \mathbf{m}) = \\ & = [\alpha_s] \int [dp_a] \left(-\frac{1}{\epsilon} \right) \left(\frac{4E_a^2}{\mu^2} \right)^{-\epsilon} \frac{\Gamma^2(1 - \epsilon)}{\Gamma(1 - 2\epsilon)} \int_{z_{\min}}^1 dz (1 - z)^{-2\epsilon} \left[\frac{P_{qq}(z)}{z} F_{\text{LM}}(z \cdot a_q) - \frac{2C_F}{1 - z} F_{\text{LM}}(a_q) \right]. \end{aligned} \quad (2.33)$$

According to the momentum conservation constraint in Eq. 1.4, E_{\max} must be greater than or equal to the maximum energy that a final-state parton can carry. Consequently, $E_{\max} \geq E_a$ and thus $z_{\min} \leq 0$. This implies that $F_{\text{LM}}(z \cdot a_q) = 0$ for $z \in [z_{\min}, 0]$, while the second term on the right-hand side of Eq. 2.35 extends all the way down to z_{\min} . Furthermore, in P_{qq} , we isolate the term that is singular in the $z \rightarrow 1$ limit in the following way

$$P_{qq}(z) = \frac{2C_F}{1 - z} + P_{qq,\text{reg}}(z), \quad P_{qq,\text{reg}}(z) = -C_F[(1 + z) + \epsilon(1 - z)], \quad (2.34)$$

and write

$$\begin{aligned} & \int [dp_{\mathbf{m}}] \int [dp_a] C_{am} \bar{S}_{\mathbf{m}} \Delta^{(\mathbf{m})} F_{\text{LM}}(a_q, \mathbf{m}) = \\ & = -\frac{[\alpha_s]}{\epsilon} \int [dp_a] \left(\frac{2E_a}{\mu} \right)^{-2\epsilon} \frac{\Gamma^2(1 - \epsilon)}{\Gamma(1 - 2\epsilon)} \left\{ \int_0^1 dz \left[\left(\frac{2C_F}{(1 - z)^{1+2\epsilon}} + \frac{P_{qq,\text{reg}}(z)}{(1 - z)^{2\epsilon}} \right) \times \right. \right. \\ & \quad \times \left. \frac{F_{\text{LM}}(z \cdot a_q)}{z} - \frac{2C_F}{(1 - z)^{1+2\epsilon}} F_{\text{LM}}(a_q) \right] + C_F \frac{(E_{\max}/E_a)^{-2\epsilon} - 1}{\epsilon} F_{\text{LM}}(a_q) \left. \right\}. \end{aligned} \quad (2.35)$$

Now we identify $G(z) = F_{\text{LM}}(z \cdot a_q)/z$, and use the definition of the plus distribution

$$\frac{1}{(1 - z)^{1+2\epsilon}} = \sum_{n=0}^{\infty} \frac{(-2\epsilon)^n \log^n(1 - z)}{n! (1 - z)}, \quad (2.36)$$

and the following equation

$$\int_0^1 dz \mathcal{D}_n(z) G(z) = \int_0^1 dz \frac{\log^n(1-z)}{1-z} (G(z) - G(1)) , \quad (2.37)$$

and we get

$$\begin{aligned} & \int [dp_{\mathbf{m}}] \int [dp_a] C_{a\mathbf{m}} \bar{S}_{\mathbf{m}} \Delta^{(\mathbf{m})} F_{\text{LM}}(a_q, \mathbf{m}) = \\ & = -\frac{[\alpha_s]}{\epsilon} \int [dp_a] \left(\frac{2E_a}{\mu} \right)^{-2\epsilon} \frac{\Gamma^2(1-\epsilon)}{\Gamma(1-2\epsilon)} \left\{ \int_0^1 \frac{dz}{(1-z)^{2\epsilon}} P_{qq, \text{reg}}(z) \frac{F_{\text{LM}}(z \cdot a_q)}{z} + \right. \\ & \left. + 2C_F \sum_{n=0}^{\infty} \frac{(-2\epsilon)^n}{n!} \int_0^1 dz \mathcal{D}_n(z) \frac{F_{\text{LM}}(z \cdot a_q)}{z} + \int_0^1 C_F \frac{(E_{\text{max}}/E_a)^{-2\epsilon} - 1}{\epsilon} F_{\text{LM}}(a_q) \right\} . \end{aligned} \quad (2.38)$$

Moreover, we introduce the following definition

$$\hat{P}_{qq}^{(0)}(z) = C_F \left[2\mathcal{D}_0(z) - (1+z) + \frac{3}{2}\delta(1-z) \right] , \quad (2.39)$$

that is the Leading-Order Altarelli-Parisi splitting kernel, and

$$\mathcal{P}_{qq}^{\text{fin}} = -\frac{C_F}{\epsilon} \left[2 \sum_{n=1}^{\infty} \frac{(-2\epsilon)^n}{n!} \mathcal{D}_n(z) + (1-z)^{-2\epsilon} P_{qq, \text{reg}}(z) + (1-z) \right] . \quad (2.40)$$

These definitions appear in the definition of the *generalized splitting function*, which allows us to express the result in a more compact form.

$$\mathcal{P}_{qq}^{\text{gen}} = \left(\frac{2E_a}{\mu} \right)^{-2\epsilon} \frac{\Gamma^2(1-\epsilon)}{\Gamma(1-2\epsilon)} \left[-P_{qq}^{(0)} + \epsilon \mathcal{P}_{qq}^{\text{fin}} \right] . \quad (2.41)$$

It is also useful to introduce the *generalized initial-state anomalous dimension*, which reads

$$\Gamma_{a,q} = \left(\frac{2E_a}{\mu} \right)^{-2\epsilon} \frac{\Gamma^2(1-\epsilon)}{\Gamma(1-2\epsilon)} \left(\gamma_q + \vec{T}_q^2 \frac{1 - e^{-2\epsilon L_a}}{\epsilon} \right) , \quad (2.42)$$

where γ_q is the anomalous dimension of the initial-state parton $a = q$, which can be found in Appendix A.2, and $L_a = \log(E_{\text{max}}/E_a)$. Therefore, the integrated soft-collinear counterterm for a gluon going collinear to a quark a in the initial state reads

$$\langle C_{a\mathbf{m}} \bar{S}_{\mathbf{m}} \Delta^{(\mathbf{m})} F_{\text{LM}}(\mathbf{m}) \rangle = [\alpha_s] \left\langle \frac{\Gamma_{a,q}}{\epsilon} F_{\text{LM}} \right\rangle + \frac{[\alpha_s]}{\epsilon} \langle \mathcal{P}_{qq}^{\text{gen}} \otimes F_{\text{LM}} \rangle , \quad (2.43)$$

where we also used the shorthand notation

$$\mathcal{P}_{qq}^{\text{gen}} \otimes F_{\text{LM}} = \int_0^1 dz \mathcal{P}_{qq}^{\text{gen}}(z) \frac{F_{\text{LM}}(z \cdot a_q)}{z} . \quad (2.44)$$

Let us now consider the situation where a final-state gluon \mathbf{m} becomes collinear with an initial-state gluon a . The calculation remains analogous to the previous case, but the form of some

functions changes. Specifically, the splitting function is now P_{gg} , whose expression is given in Eq. A.10. Furthermore, the leading-order Altarelli-Parisi splitting kernel is now $\hat{P}_{gg}^{(0)}(z)$, reported in A.12. The integrated soft-collinear counterterm in this case has the same form as in Eq. 2.43, but uses the generalized anomalous dimension for a gluon $\Gamma_{a,g}$ (defined as in 2.42, with g in place of q), and the term from Eq. 2.44 now involves the generalized splitting function $\mathcal{P}_{gg}^{\text{gen}}$. This function has the form 2.41, adapted for the case of a gluon collinear to another gluon.

Finally, we consider the case where a final-state quark \mathbf{m} becomes collinear with another initial-state parton a , which can be either a quark or a gluon. As stated previously, quarks do not give rise to soft singularities. Therefore, in this scenario, the term involving the anomalous dimension in Eq. 2.43 is absent. Only the term from Eq. 2.44 remains, which is connected to the splitting functions P_{qg} and P_{gq} given in A.10, and to the Altarelli-Parisi splitting kernels $\hat{P}_{qg}^{(0)}$ and $\hat{P}_{gq}^{(0)}$ listed in A.12.

§2.6.2 Final state

Let us now consider a situation where a final-state gluon \mathbf{m} becomes collinear with another final-state gluon i . This can occur, for example, in the case of the $\mathcal{P}_2^{\text{NLO}}$ process. In this case, the function F_{FL} depends on the energy fraction $z = 1 - E_{\mathbf{m}}/E_{[i\mathbf{m}]} = E_i/E_{[i\mathbf{m}]}$, and, under the action of the collinear operator, it factorizes in the following way

$$C_{i\mathbf{m}}\Delta^{(\mathbf{m})}F_{\text{LM}}(\mathbf{m}) = \frac{g_{s,b}^2}{p_i \cdot p_{\mathbf{m}}} z P_{gg}(z) F_{\text{LM}}(i\mathbf{m}), \quad (2.45)$$

where the argument of the function F_{LM} on the right-hand side shows the dependence on the momentum of the single final-state gluon $[i\mathbf{m}]$ resulting from the merging of the two collinear gluons, and

$$P_{gg}(z) = 2C_A \left[\frac{z}{1-z} + \frac{1-z}{z} + z(1-z) \right] \equiv P_{qq}(1-z). \quad (2.46)$$

We perform the integration in hyperspherical coordinates over the phase space of the gluons involved in the collinear limit, namely i and \mathbf{m} . To facilitate the subsequent change of variables, we isolate, from the angular integral, the integration over the relative angle between partons i and \mathbf{m} , i.e., $\theta_{[i\mathbf{m}]}$, and in particular we highlight the variable $\eta_{i\mathbf{m}} = \rho_{i\mathbf{m}}/2$

$$\begin{aligned} \int [dp_i] \int [dp_{\mathbf{m}}] C_{i\mathbf{m}}\Delta^{(\mathbf{m})}F_{\text{LM}} &= \\ &= \int \frac{d\Omega^{d-2}}{2(2\pi)^{d-1}} 2^{-2\epsilon} \int_0^1 \frac{d\eta_{i\mathbf{m}}}{(\eta_{i\mathbf{m}}(1-\eta_{i\mathbf{m}}))^\epsilon} \int [d\Omega_i] \int dE_{\mathbf{m}} E_{\mathbf{m}}^{1-2\epsilon} \int dE_i E_i^{1-2\epsilon} \frac{g_{s,b}^2 P_{gg} F_{\text{LM}}(i\mathbf{m})}{(1-z) E_{i\mathbf{m}}^2 \eta_{i\mathbf{m}}}. \end{aligned} \quad (2.47)$$

We now employ the following integrals

$$\int \frac{d\Omega^{d-2}}{2(2\pi)^{d-1}} = \frac{1}{8\pi^2} \frac{(4\pi)\epsilon}{\Gamma(1-\epsilon)}, \quad (2.48)$$

and

faccio i conti, mostro che non ottengo la consueta generalised final-state anomalous dimension, ma devo sommare i casi per ottenerla.

Discorso generale su come ottengo operatore I_C nell'initial state e nel final state, e in generale che forma hanno le correzioni in questo caso.

Operator I_C

$$I_C(\epsilon) = \sum_{i=1}^{N_p} \frac{\Gamma_{i,f_i}}{\epsilon} \quad (2.49)$$

§2.7 Cancellation of poles

Chapter 3

NLO QCD corrections with θ -parameters in the NSC Subtraction Scheme

Il lavoro esposto nel capitolo precedente può essere ulteriormente generalizzato, come è stato fatto nei paper [19, 21]. In questo capitolo ripercorriamo tali risultati, implementando theta parameters. Lo facciamo perché uno dei principali difetti di NSC SS è che la sua efficienza è un po' impattata dalla numerical integration of the subtraction terms.

§3.1 Draft

Soft limit

$$\langle S_m^{\theta_s} F_{\text{LM}}(\mathbf{m}) \rangle = \int [dp_m] \theta(E_m < \theta_s E_{\text{max}}) (-g_{s,b}^2) \sum_{(ij)}^{N_p} \frac{p_i \cdot p_j}{(p_i \cdot p_m)(p_j \cdot p_m)} (\vec{T}_i \cdot \vec{T}_j) F_{\text{LM}} \quad (3.1)$$

$$\langle S_m^{\theta_s} F_{\text{LM}}(\mathbf{m}) \rangle = -[\alpha_s] \frac{(2E_{\text{max}}/\mu)^{-2\epsilon}}{\epsilon^2} \theta_s^{-2\epsilon} \sum_{(ij)}^{N_p} \langle \eta_{(ij)}^{-\epsilon} K_{ij}(\vec{T}_i \cdot \vec{T}_j) \cdot F_{\text{LM}} \rangle \quad (3.2)$$

$$\begin{aligned} &= \frac{1}{\epsilon^2} \sum_{i=1}^{N_p} T_i^2 + \frac{1}{\epsilon} \left[- \sum_{i=1}^{N_p} 2 \log \left(\frac{2E_{\text{max}} \theta_s}{\mu} \right) \vec{T}_i^2 - \sum_{i \neq j}^{N_p} f_1(\eta_{ij}) (\vec{T}_i \cdot \vec{T}_j) \right] + \\ &+ \sum_{i=1}^{N_p} 2 \log^2 \left(\frac{2E_{\text{max}} \theta_s}{\mu} \right) \vec{T}_i^2 - \sum_{i \neq j}^{N_p} \left[f_2(2E_{\text{max}} \theta_s) f_1(\eta_{ij}) + K_{ij}^{(2)} \right] (\vec{T}_i \cdot \vec{T}_j) + \mathcal{O}(\epsilon) \end{aligned} \quad (3.3)$$

Coefficient

$$\begin{aligned} c_{-1}(\theta_s) &= - \sum_{i=1}^{N_p} 2 \log \left(\frac{2E_{\text{max}} \theta_s}{\mu} \right) \vec{T}_i^2 - \sum_{i \neq j}^{N_p} f_1(\eta_{ij}) (\vec{T}_i \cdot \vec{T}_j) = \\ &= - \sum_{i=1}^{N_p} \left(2\text{Li}^{\theta_s} + 2 \log \left(\frac{2E_i}{\mu} \right) \right) \vec{T}_i^2 - \sum_{i \neq j}^{N_p} f_1(\eta_{ij}) (\vec{T}_i \cdot \vec{T}_j) \end{aligned} \quad (3.4)$$

Final state

Collinear limit

$$\langle C_{im}^{\theta_i} \Delta^m F_{\text{LM}}(\mathbf{m}) \rangle = \int \dots \int [dp_i] \int [dp_m] \frac{g_{s,b}^2}{p_i \cdot p_m} z P_{gg}(z) F_{\text{LM}}(im) \quad (3.5)$$

$$\langle C_{i\mathbf{m}}^{\theta_i} \Delta^{\mathbf{m}} F_{\text{LM}}(\mathbf{m}) \rangle = [\alpha_s] [\mathrm{d}\eta_{i\mathbf{m}\theta_i}] \int \dots \int [\mathrm{d}p_i] \left(\frac{2E_i}{\mu} \right)^{-2\epsilon} \int_0^1 \mathrm{d}z z^{1-2\epsilon} (1-z)^{-2\epsilon} P_{gg}(z) F_{\text{LM}} \quad (3.6)$$

$$\begin{aligned} \langle C_{i\mathbf{m}}^{\theta_i} \bar{S}_{\mathbf{m}}^{\theta_s} \Delta^{\mathbf{m}} F_{\text{LM}}(\mathbf{m}) \rangle = [\alpha_s] \langle \left\{ \frac{1}{\epsilon} (\gamma_g + 2\vec{T}_g^2 \text{Li}^{\theta_s}) - 2 \log \frac{2E_i}{\mu} \gamma_g + \right. \\ \left. - 4 \log \frac{2E_i}{\mu} \vec{T}_g^2 \text{Li}^{\theta_s} - \log \theta_i \gamma_g - 2\vec{T}_g^2 \text{Li}^{\theta_s} \log \theta_i \right\} F_{\text{LM}} \rangle \end{aligned} \quad (3.7)$$

Appendices

Appendix A

Useful definitions

§A.1 Constants

We report in this section useful constants that are used throughout the thesis. We denote the color-charge operators by \vec{T}_i , whose square gives the Casimir operator of the corresponding representation of $SU(3)$, and identifies the color charge of the represented parton. If N_c is the number of colors, we have

$$\vec{T}_q^2 = \vec{T}_{\bar{q}}^2 = C_F = \frac{N_c^2 - 1}{2N_c}, \quad \vec{T}_g^2 = C_A = N_c. \quad (\text{A.1})$$

The expressions for quark and gluons anomalous dimensions are

$$\gamma_q = \frac{3}{2}C_F \quad \gamma_g = \frac{11}{6}C_A - \frac{2}{3}T_R n_f, \quad (\text{A.2})$$

where $T_R = 1/2$, and n_f is the number of massless quarks flavors. Moreover, we introduce the following shorthand

$$[\alpha_s] = \frac{\alpha_s(\mu)}{2\pi} \frac{e^{\epsilon\gamma_E}}{\Gamma(1-\epsilon)}, \quad (\text{A.3})$$

with $\alpha_s(\mu)$ the running coupling constant, and γ_E the Euler-Mascheroni constant.

§A.2 Partitions at NLO

To manage the calculation of QCD corrections for processes with many final-state particles, we introduce partitions that separate resolved and potentially unresolved partons. Following the construction proposed in [19], we consider a process with N_p partons at leading order and an arbitrary colorless final state

$$f_1(p_1) + f_2(p_2) \rightarrow f_3(p_3) + \cdots + f_{N_p}(p_{N_p}) + X. \quad (\text{A.4})$$

At NLO, we add an extra parton to the final state, in order to describe the real-emission process. The list of the $N = N_p - 2$ final-state partons becomes $\mathcal{H}_f = \{f_3, f_4, \dots, f_{N_p}, f_{N_p+1}\}$. If parton i becomes unresolved, we denote the set of $N + 1$ final-state partons as $\mathcal{H}_f^{(i)}$, where $\mathcal{H}_f^{(i)} = \mathcal{H}_f / \{i\}$, and we introduce the function

$$d^{(i)} = \prod_{k \in \mathcal{H}_f^{(i)}} p_{k,\perp} \prod_{l < m \in \mathcal{H}_f^{(i)}} (1 - \cos \theta_{lm}), \quad (\text{A.5})$$

where $p_{k,\perp}$ is the transverse momentum of parton k .

Using the functions in Eq. A.5, we can construct the partitions

$$\Delta^{(i)} = \frac{d^{(i)}}{\sum_{j \in \mathcal{H}_f} d^{(j)}}, \quad (\text{A.6})$$

where $i \in \mathcal{H}_f$. Starting from their definition, it is straightforward to demonstrate that the partition functions form a partition of unity

$$\sum_{i \in \mathcal{H}_f} \Delta^{(i)} = 1. \quad (\text{A.7})$$

If we act with the soft operator S_k on the function $\Delta^{(i)}$, we get

$$S_k \Delta^{(i)} = \delta_{ki}. \quad (\text{A.8})$$

Instead, if we act with the collinear operator C_{lm} , i.e., when partons l and m become collinear, we get

$$C_{lm} \Delta^{(i)} = \begin{cases} 0, & l, m \neq i, \\ 1, & l = i, m \in 1, 2, \\ z_{i,m}, & l = i, m \in \mathcal{H}_f^{(i)}, \end{cases} \quad (\text{A.9})$$

with $z_{i,m} = \frac{E_m}{E_i + E_m}$, and partons 1 and 2 in the initial state.

§A.3 Splitting functions

A splitting function describes the probability that a high-energy parton will split into two other partons. There are two main types of splittings: final-state and initial-state. In a final-state splitting, a parton produced in a collision splits after the main interaction. We write this process as $[i\mathbf{m}]^* \rightarrow i(z) + \mathbf{m}(1-z)$, where $[i\mathbf{m}]$ is the original “mother” parton, i and \mathbf{m} are the two new “daughter” partons, z is the fraction of the mother’s energy carried by parton i , defined as $z = 1 - E_{\mathbf{m}}/E_{[i\mathbf{m}]}$. The probability for this splitting is given by the spin-averaged *final-state splitting function*, $P_{f_{[i\mathbf{m}]f_i}}(z)$. Its form depends on whether the partons involved are quarks (q) or gluons (g). The functions are

$$\begin{aligned} P_{qq}(z) &= C_F \left[\frac{1+z^2}{1-z} - \epsilon(1-z) \right], \\ P_{gg}(z) &= 2C_A \left[\frac{z}{1-z} + \frac{1-z}{z} + z(1-z) \right] \equiv P_{qq}(1-z), \\ P_{qg}(z) &= T_R \left[1 - \frac{2z(1-z)}{1-\epsilon} \right], \\ P_{gq}(z) &= 2C_A \left[\frac{z}{1-z} + \frac{1-z}{z} + z(1-z) \right]. \end{aligned} \quad (\text{A.10})$$

In an initial-state splitting, a parton coming from one of the colliding protons radiates another parton before the main collision. We write this as $i \rightarrow [i\mathbf{m}]^* + \mathbf{m}$, where i is the initial incoming

parton from the proton, $[i\mathbf{m}]$ is the parton that enters the hard scattering, \mathbf{m} is the radiated parton, and z is the fraction of the initial parton's energy taken into the hard process, $z = 1 - E_{\mathbf{m}}/E_i$. The probability for this is given by the *initial-state splitting function*, $P_{f_{[i\mathbf{m}]}f_i,i}(z)$. These functions are not independent; they are directly related to the final-state ones by the following relations

$$\begin{aligned}
P_{qq,i}(z) &= -zP_{qq}(1/z) \equiv P_{qq}(z), \\
P_{qg,i}(z) &= \left[\frac{2N_c}{2(1-\epsilon)(N_c^2-1)} \right] zP_{qg}(1/z) \equiv P_{qg}, \\
P_{gq,i}(z) &= \left[\frac{2(1-\epsilon)(N_c^2-1)}{2N_c} \right] zP_{gq}(1/z) \equiv P_{gq}(z), \\
P_{gg,i}(z) &= -zP_{gg}(1/z) \equiv P_{gg}(z).
\end{aligned} \tag{A.11}$$

Finally, for reference, we also use the conventional leading-order Altarelli-Parisi splitting functions [5]. They are written as

$$\begin{aligned}
\hat{P}_{qq}^{(0)}(z) &= C_F \left[2\mathcal{D}_0(z) - (1+z) + \frac{3}{2}\delta(1-z) \right], \\
\hat{P}_{qg}^{(0)}(z) &= T_R \left[(1-z)^2 + z^2 \right], \\
\hat{P}_{gq}^{(0)}(z) &= C_F \left[\frac{1 + (1-z)^2}{z} \right], \\
\hat{P}_{gg}^{(0)}(z) &= 2C_A \left[\mathcal{D}_0(z) + z(1-z) + \frac{1}{z} - 2 \right] + \beta_0\delta(1-z).
\end{aligned} \tag{A.12}$$

Bibliography

- [1] F. Bloch and A. Nordsieck. “Note on the Radiation Field of the Electron”. *Phys. Rev.* **52** (1937), pp. 54–59. DOI: [10.1103/PhysRev.52.54](https://doi.org/10.1103/PhysRev.52.54).
- [2] G. 't Hooft. “Dimensional regularization and the renormalization group”. *Nuclear Physics B* **61** (1973), pp. 455–468. ISSN: 0550-3213. DOI: [https://doi.org/10.1016/0550-3213\(73\)90376-3](https://doi.org/10.1016/0550-3213(73)90376-3).
- [3] Guido Altarelli and G. Parisi. “Asymptotic Freedom in Parton Language”. *Nucl. Phys. B* **126** (1977), pp. 298–318. DOI: [10.1016/0550-3213\(77\)90384-4](https://doi.org/10.1016/0550-3213(77)90384-4).
- [4] John C. Collins and Davison E. Soper. “The Theorems of Perturbative QCD”. *Ann. Rev. Nucl. Part. Sci.* **37** (1987), pp. 383–409. DOI: [10.1146/annurev.ns.37.120187.002123](https://doi.org/10.1146/annurev.ns.37.120187.002123).
- [5] R. K. Ellis et al. *QCD and Collider Physics*. **8**. Cambridge Monographs on Particle Physics, Nuclear Physics and Cosmology. Cambridge: Cambridge University Press, 1996, p. 435. DOI: [10.1017/CB09780511628788](https://doi.org/10.1017/CB09780511628788).
- [6] S. Frixione, Z. Kunszt, and A. Signer. “Three jet cross-sections to next-to-leading order”. *Nucl. Phys. B* **467** (1996), pp. 399–442. DOI: [10.1016/0550-3213\(96\)00110-1](https://doi.org/10.1016/0550-3213(96)00110-1). arXiv: [hep-ph/9512328](https://arxiv.org/abs/hep-ph/9512328).
- [7] S. Catani and M. H. Seymour. “A General algorithm for calculating jet cross-sections in NLO QCD”. *Nucl. Phys. B* **485** (1997). [Erratum: *Nucl. Phys. B* 510, 503–504 (1998)], pp. 291–419. DOI: [10.1016/S0550-3213\(96\)00589-5](https://doi.org/10.1016/S0550-3213(96)00589-5). arXiv: [hep-ph/9605323](https://arxiv.org/abs/hep-ph/9605323).
- [8] Stefano Catani. “The Singular behavior of QCD amplitudes at two loop order”. *Phys. Lett. B* **427** (1998), pp. 161–171. DOI: [10.1016/S0370-2693\(98\)00332-3](https://doi.org/10.1016/S0370-2693(98)00332-3). arXiv: [hep-ph/9802439](https://arxiv.org/abs/hep-ph/9802439).
- [9] Stefano Catani and Massimiliano Grazzini. “Infrared factorization of tree level QCD amplitudes at the next-to-next-to-leading order and beyond”. *Nucl. Phys. B* **570** (2000), pp. 287–325. DOI: [10.1016/S0550-3213\(99\)00778-6](https://doi.org/10.1016/S0550-3213(99)00778-6). arXiv: [hep-ph/9908523](https://arxiv.org/abs/hep-ph/9908523).
- [10] Gavin P. Salam. “Towards Jetography”. *Eur. Phys. J. C* **67** (2010), pp. 637–686. DOI: [10.1140/epjc/s10052-010-1314-6](https://doi.org/10.1140/epjc/s10052-010-1314-6). arXiv: [0906.1833](https://arxiv.org/abs/0906.1833) [[hep-ph](https://arxiv.org/abs/hep-ph)].
- [11] Stefan Höche. “Introduction to parton-shower event generators”. arXiv preprint [arXiv:1411.4085](https://arxiv.org/abs/1411.4085) (2014). Lectures presented at TASI 2014. 40 pages, 12 figures. URL: <https://arxiv.org/abs/1411.4085>.
- [12] Fabrizio Caola, Kirill Melnikov, and Raoul Röntsch. “Nested soft-collinear subtractions in NNLO QCD computations”. *Eur. Phys. J. C* **77.4** (2017), p. 248. DOI: [10.1140/epjc/s10052-017-4774-0](https://doi.org/10.1140/epjc/s10052-017-4774-0). arXiv: [1702.01352](https://arxiv.org/abs/1702.01352) [[hep-ph](https://arxiv.org/abs/hep-ph)].

- [13] John Campbell, Joey Huston, and Frank Krauss. *The Black Book of Quantum Chromodynamics : a Primer for the LHC Era*. Oxford University Press, 2018. DOI: [10.1093/oso/9780199652747.001.0001](https://doi.org/10.1093/oso/9780199652747.001.0001).
- [14] K. Melnikov. “Lectures on QCD for hadron colliders”. *Proceedings of the 2017 European School of High-Energy Physics, Evora, Portugal, 6–19 September 2017*. Ed. by M. Mulders and G. Zanderighi. Vol. 3/2018. CERN Yellow Reports: School Proceedings. CERN-2018-006-SP. Geneva: CERN, 2018. DOI: [10.23730/CYRSP-2018-003.37](https://doi.org/10.23730/CYRSP-2018-003.37).
- [15] Fabrizio Caola, Kirill Melnikov, and Raoul Röntsch. “Analytic results for color-singlet production at NNLO QCD with the nested soft-collinear subtraction scheme”. *Eur. Phys. J. C* **79**.5 (2019), p. 386. DOI: [10.1140/epjc/s10052-019-6880-7](https://doi.org/10.1140/epjc/s10052-019-6880-7). arXiv: [1902.02081](https://arxiv.org/abs/1902.02081) [hep-ph].
- [16] Fabrizio Caola, Kirill Melnikov, and Raoul Röntsch. “Analytic results for decays of color singlets to gg and $q\bar{q}$ final states at NNLO QCD with the nested soft-collinear subtraction scheme”. *Eur. Phys. J. C* **79**.12 (2019), p. 1013. DOI: [10.1140/epjc/s10052-019-7505-x](https://doi.org/10.1140/epjc/s10052-019-7505-x). arXiv: [1907.05398](https://arxiv.org/abs/1907.05398) [hep-ph].
- [17] K. Asteriadis. “Application of the nested soft-collinear subtraction scheme to the description of deep inelastic scattering”. PhD Thesis. Karlsruhe Institute of Technology (KIT), Institute for Experimental Particle Physics (EKP), 24, 2020, p. 216. DOI: [10.5445/IR/1000135340](https://doi.org/10.5445/IR/1000135340).
- [18] Konstantin Asteriadis et al. “Analytic results for deep-inelastic scattering at NNLO QCD with the nested soft-collinear subtraction scheme”. *Eur. Phys. J. C* **80**.1 (2020), p. 8. DOI: [10.1140/epjc/s10052-019-7567-9](https://doi.org/10.1140/epjc/s10052-019-7567-9). arXiv: [1910.13761](https://arxiv.org/abs/1910.13761) [hep-ph].
- [19] Federica Devoto et al. “A fresh look at the nested soft-collinear subtraction scheme: NNLO QCD corrections to N-gluon final states in $q\bar{q}$ annihilation”. *JHEP* **02** (2024), p. 016. DOI: [10.1007/JHEP02\(2024\)016](https://doi.org/10.1007/JHEP02(2024)016). arXiv: [2310.17598](https://arxiv.org/abs/2310.17598) [hep-ph].
- [20] Federica Devoto et al. “Integrated subtraction terms and finite remainders for arbitrary processes with massless partons at colliders in the nested soft-collinear subtraction scheme” (2025). arXiv: [2509.08594](https://arxiv.org/abs/2509.08594) [hep-ph].
- [21] Federica Devoto et al. “Towards a general subtraction formula for NNLO QCD corrections to processes at hadron colliders: final states with quarks and gluons”. *JHEP* **08** (2025), p. 122. DOI: [10.1007/JHEP08\(2025\)122](https://doi.org/10.1007/JHEP08(2025)122). arXiv: [2503.15251](https://arxiv.org/abs/2503.15251) [hep-ph].